ECCOMAS Congress 2016
VII European Congress on Computational Methods in Applied Sciences and Engineering
M. Papadrakakis, V. Papadopoulos, G. Stefanou, V. Plevris (eds.)
Crete Island, Greece, 5–10 June 2016

ENERGY STABLE HIGH ORDER FINITE DIFFERENCE METHODS ON STAGGERED GRIDS: AN INITIAL INVESTIGATION

Ossian O'Reilly[1,2], Tomas Lundquist[2], and Jan Nordström[2]

[1]Department of Geophysics
Stanford University, CA 94305-2215
e-mail: ooreilly@stanford.edu

[2] Department of Mathematics, Division of Computational Mathematics
Linköping University, SE-581 83 Linköping, Sweden
e-mail: {tomas.lundquist,jan.nordstrom}@liu.se

Keywords: Staggered Grids, High Order Finite Difference Methods, Summation-By-Parts, Weak Boundary Conditions , Energy stability, Wave Equations.

Abstract. *We consider wave equations in first-order form and derive provably stable, high order finite difference operators on staggered grids. This is the first time that stability has been proven for initial boundary value problems for wave equations on staggered grids. The staggered grid operators are in summation-by-parts form and when combined with weak boundary conditions, lead to an energy stable scheme. Numerical computations for the two dimensional acoustic wave equation in Cartesian geometries corroborate the theoretical developments.*

1 INTRODUCTION

High order finite difference methods are highly effective for wave propagation over long distances. In particular for electromagnetic and elastic wave propagation, staggered spatial schemes perform very well [5]. Arguably the most significant challenge in a staggered grid finite difference formulation is the implementation of boundary and interface conditions at curved boundaries and material discontinuities [8]. The curved boundary is often approximated using a stair-cased grid approximation, which results in at most first-order accuracy. An alternative strategy is to conform to the boundary geometry using a curvilinear coordinate transformation. However, unless the resulting spatial discretization is energy conserving, instabilities can develop.

The curvilinear coordinate transformation technique works exceptionally well for high order finite difference methods on nodal grids that combine summation-by-parts (SBP) operators [3, 6, 11] and weak boundary conditions using the simultaneous approximation term (SAT) method [2]. The SBP-SAT approach leads to a provably stable multiblock scheme, even for highly skewed grids (provided that the Jacobian of the coordinate transformation is not ill-conditioned). So far, the SBP-SAT approach has only been applied on nodal grids. Thus, the motivation for this work is to develop a provably stable curvilinear multiblock scheme on staggered grids. As a first step toward this goal, we formulate the SBP-SAT approach on staggered grids in Cartesian geometries and construct corresponding SBP operators of the first derivative. To the best of our knowledge, this is the first time that stability has been proven for a high order finite difference method on a staggered grid for initial boundary value problems for wave equations.

2 DEFINITIONS

We begin by discretizing the interval $[\alpha\ \beta] \in \mathbb{R}$ using a nodal grid $\mathbf{x}_+$ and a cell-centered grid $\mathbf{x}_-$ (see e.g, [7]) . The grids are given by $\mathbf{x}_+ = (x_0,\ x_1,\ \ldots, x_N)^T \in \mathbb{R}^{N+1}$ and $\mathbf{x}_- = \left(x_0,\ x_{1/2},\ x_{3/2},\ \ldots,\ x_{N-1/2},\ x_N\right)^T \in \mathbb{R}^{N+2}$, where

$$x_j = \alpha + j\Delta x,\ 0 \leq j \leq N,\ x_{j-1/2} = \alpha + (j-1/2)\Delta x,\ 1 \leq j \leq N,$$

and $\Delta x = (\beta - \alpha)/N$ is the grid spacing (Figure 1). Note that both grids share the same boundary points.

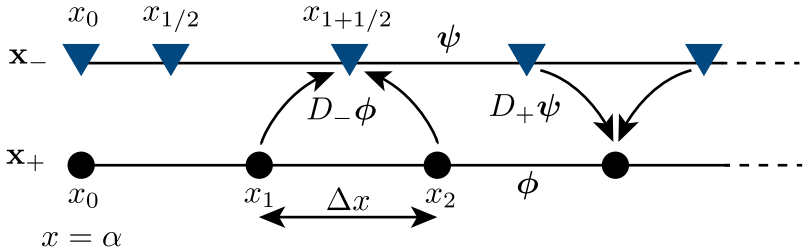

Figure 1: Nodal grid $\mathbf{x}_+$ and cell-centered grid $\mathbf{x}_-$. Both grids share the same boundary points. The difference operator D_- acts on a grid function ϕ defined on the nodal grid $\mathbf{x}_+$ and stores the result on the cell-centered grid $\mathbf{x}_-$, D_+ acts on a grid function ψ defined on the cell-centered grid $\mathbf{x}_-$ and stores the result on the nodal grid $\mathbf{x}_+$.

SBP staggered grid operators employ a high order, central finite difference approximation at each interior grid point, and one-sided difference approximations near the boundary. For

example, 2^{nd}-order accuracy in the interior is given by the standard central approximation

$$\left.\frac{d\psi}{dx}\right|_{x_i} \approx \frac{\psi_{i+1/2}-\psi_{i-1/2}}{\Delta x},\ \left.\frac{d\phi}{dx}\right|_{x_{i-1/2}} \approx \frac{\phi_i-\phi_{i-1}}{\Delta x},$$

for smooth grid functions $\boldsymbol{\psi}$ and $\boldsymbol{\phi}$ defined on $\mathbf{x}_-$ and $\mathbf{x}_+$, respectively. The SBP staggered grid operators are defined by

$$D_+ = P_+^{-1}Q_+ \in \mathbb{R}^{(N+1)\times(N+2)},\quad D_- = P_-^{-1}Q_- \in \mathbb{R}^{(N+2)\times(N+1)},$$

where $P_+ \in \mathbb{R}^{(N+1)\times(N+1)}$, $Q_+ \in \mathbb{R}^{(N+1)\times(N+2)}$, $P_- \in \mathbb{R}^{(N+2)\times(N+2)}$, $Q_- \in \mathbb{R}^{(N+2)\times(N+1)}$. Here, D_+ acts on grid functions defined on $\mathbf{x}_-$ and D_- acts on grid functions defined on $\mathbf{x}_+$. The way that D_+, D_- acts on $\mathbf{x}_-$, $\mathbf{x}_+$ and store the result is schematically shown in Figure 1, for the 2^{nd}-order accurate case. For an order of accuracy q we have the relations

$$D_+\boldsymbol{\psi}^k = k\boldsymbol{\phi}^{k-1},\ D_-\boldsymbol{\phi}^k = k\boldsymbol{\psi}^{k-1},\ k=0,1,\ldots,q,$$

where $\boldsymbol{\phi}^k$ denotes the k^{th}-monomial (each component of the vector is raised to the k^{th}-power). In the interior the accuracy is $q=2s$ and for points near the boundary it is $q=s$. In addition, the SBP staggered grid operators satisfy:

(i) P_+ and P_- are symmetric and positive definite matrices defining the respective discrete L_2 norms

$$\|\boldsymbol{\phi}\|_{h+}^2 = \boldsymbol{\phi}^T P_+ \boldsymbol{\phi} \approx \int_\alpha^\beta \phi^2 dx,\ \|\boldsymbol{\psi}\|_{h-}^2 = \boldsymbol{\psi}^T P_- \boldsymbol{\psi} \approx \int_\alpha^\beta \psi^2 dx.$$

(ii) The matrices Q_+ and Q_- satisfy the SBP property

$$Q_+ + Q_-^T = B_+ = B_-^T = \mathbf{e}_{N+}\mathbf{e}_{N-}^T - \mathbf{e}_{0+}\mathbf{e}_{0-}^T \in \mathbb{R}^{(N+1)\times(N+2)}. \tag{1}$$

In (1), the vectors $\mathbf{e}_{0\pm}$,$\mathbf{e}_{N\pm}$ are of appropriate sizes, and gathers the value at each boundary point, i.e.,

$$\mathbf{e}_{0+}^T\mathbf{x}_+ = \mathbf{e}_{0-}^T\mathbf{x}_- = \alpha,\ \mathbf{e}_{N+}^T\mathbf{x}_+ = \mathbf{e}_{N-}^T\mathbf{x}_- = \beta. \tag{2}$$

For example, a pair of 2^{nd}-order SBP staggered grid operators are given by

$$Q_+ = \begin{pmatrix} -\frac{1}{2} & \frac{1}{4} & \frac{1}{4} & & \\ -\frac{1}{2} & -\frac{1}{4} & \frac{3}{4} & & \\ & & -1 & 1 & \\ & & & \ddots & \ddots \end{pmatrix},\ Q_- = \begin{pmatrix} -\frac{1}{2} & \frac{1}{2} & & & \\ -\frac{1}{4} & \frac{1}{4} & & & \\ -\frac{1}{4} & -\frac{3}{4} & & & \\ & & -1 & 1 & \\ & & & \ddots & \ddots \end{pmatrix}$$

and

$$P_+ = \text{diag}\left(\frac{1}{2},\ 1, 1, \ldots\right)\Delta x,\ P_- = \text{diag}\left(\frac{1}{2},\ \frac{1}{4},\ \frac{5}{4},\ 1, \ldots\right)\Delta x.$$

3 ANALYSIS

As a prototype problem, we consider the scalar wave equation in one dimension

$$u_t + Au_x = 0, \quad \alpha \leq x \leq \beta,\ t \geq 0, \quad u = \begin{pmatrix} p \\ v \end{pmatrix},\ A = \begin{pmatrix} 0 & 1 \\ 1 & 0 \end{pmatrix}, \tag{3}$$

subject to appropriate initial and boundary conditions. We apply the energy method [1] to (3), which leads to

$$\frac{d}{dt}\|u\|^2 = -u^T Au\big|_\alpha^\beta = -2pv\big|_\alpha^\beta, \tag{4}$$

where $\|u\| = \int_\alpha^\beta u^T u dx$. By considering the boundary at $x = \alpha$ only and diagonalizing

$$A = X\Lambda X^T, X = \frac{1}{\sqrt{2}}\begin{pmatrix} -1 & 1 \\ 1 & 1 \end{pmatrix},\ \Lambda = \begin{pmatrix} -1 & 0 \\ 0 & 1 \end{pmatrix} \tag{5}$$

we obtain

$$\frac{d}{dt}\|u\|^2 = w^T\Lambda w\big|_{x=\alpha} = (w^+)^2\big|_{x=\alpha} - (w^-)^2\big|_{x=\alpha},$$

where $w = (w^-, w^+)$, $w^\pm = (X^\pm)^T\mathbf{u}$ are the characteristic variables, and $\Lambda = \text{diag}(\Lambda^-, \Lambda^+)$ contain the positive and negative eigenvalues and the corresponding eigenvectors $X = (X^-, X^+)$, respectively. The linear homogeneous boundary condition

$$w^+\big|_{x=\alpha} - rw^-\big|_{x=\alpha} = 0 \tag{6}$$

leads to

$$\frac{d}{dt}\|u\|^2 = w^T\Lambda w = (r^2-1)(w^-)^2\big|_{x=\alpha}, \tag{7}$$

and we have an estimate for $|r| \leq 1$.

3.1 The semi-discrete approximation

An SBP-SAT staggered grid approximation of (3) is given by

$$\mathbf{u}_t + \tilde{A}\mathbf{u} = P^{-1}E_0\Sigma L E_0^T\mathbf{u}, \tag{8}$$

where

$$\mathbf{u} = \begin{pmatrix} \mathbf{p} \\ \mathbf{v} \end{pmatrix},\ \tilde{A} = \begin{pmatrix} 0 & D_- \\ D_+ & 0 \end{pmatrix},\ E_0 = \begin{pmatrix} \mathbf{e}_{0-} & \mathbf{0} \\ \mathbf{0} & \mathbf{e}_{0+} \end{pmatrix},\ P = \begin{pmatrix} P_- & 0 \\ 0 & P_+ \end{pmatrix},$$

and $\mathbf{p} = \big(p_0,\ p_{1/2},\ \ldots,\ p_{N-1/2},\ p_N\big)^T$ is stored on $\mathbf{x}_-$, $\mathbf{v} = (v_0,\ v_1,\ \ldots,\ v_N)^T$ is stored on $\mathbf{x}_+$. The boundary condition is weakly imposed at $x = \alpha$ with the aid of E_0^T that gathers the solution on the boundary, i.e. $\mathbf{u}_0 = E_0^T\mathbf{u} = (p_0,\ v_0)$. The boundary operator $L \in \mathbb{R}^{1\times 2}$ is given by (6), that is

$$L\mathbf{u}_0 = \big((X^+)^T - r(X^-)^T\big)\,\mathbf{u}_0 = w_0^+ - rw_0^-. \tag{9}$$

The penalty matrix $\Sigma \in \mathbb{R}^{2\times 1}$ is determined by applying the discrete energy method (see [12] for a general outline of the procedure). We have

$$\begin{aligned}\frac{d}{dt}\|\mathbf{u}\|_P^2 &= -2\mathbf{p}^T Q_- \mathbf{v} - 2\mathbf{v}^T Q_+ \mathbf{p} + \mathbf{u}_0^T(\Sigma L + L^T\Sigma^T)\mathbf{u}_0 \\ &= -2\mathbf{p}^T\left(Q_+^T + Q_-\right)\mathbf{v} + \mathbf{u}_0^T(\Sigma L + L^T\Sigma^T)\mathbf{u}_0 \\ &= -2\left(p_N v_N - p_0 v_0\right) + \mathbf{u}_0^T(\Sigma L + L^T\Sigma^T)\mathbf{u}_0, \end{aligned} \tag{10}$$

where $\|\mathbf{u}\|_P^2 = \mathbf{u}^T P \mathbf{u}$. Note that the SBP property (1) was used in the last step. We consider only the boundary $x = \alpha$ and write (10) in quadratic form

$$\frac{d}{dt}\|\mathbf{u}\|_P^2 = \mathbf{u}_0^T A \mathbf{u}_0 + \mathbf{u}_0^T(\Sigma L + L^T\Sigma^T)\mathbf{u}_0.$$

By using the diagonalization $A = X\Lambda X^T$ given in (5) and applying (9), we find

$$\frac{d}{dt}\|\mathbf{u}\|_P^2 = \mathbf{w}_0^T\Lambda\mathbf{w}_0 + \mathbf{w}_0^T X^T\Sigma(w_0^+ - r w_0^-) + (w_0^+ - r w_0^-)\Sigma^T X\mathbf{w}_0, \tag{11}$$

where $\mathbf{w}_0 = (w_0^-,\ w_0^+) = X^T\mathbf{u}_0$. Finally, the choice

$$\Sigma = -X^+\Lambda^+ \tag{12}$$

leads to

$$\frac{d}{dt}\|\mathbf{u}\|_P^2 = (r^2-1)(w_0^-)^2 - (w_0^+ - r w_0^-)^2 \leq 0, \quad |r| \leq 1.$$

The result is similar to (7), but also includes numerical dissipation that vanishes with grid refinement.

Remark 1. *The penalty matrix and boundary operator in (8) are given by*

$$\Sigma = -\frac{1}{\sqrt{2}}\begin{pmatrix} 1 \\ 1 \end{pmatrix},\ L = \frac{1}{\sqrt{2}}\begin{pmatrix} 1+r \\ 1-r \end{pmatrix}^T,$$

where (5), (9), and (12) have been used.

4 THE TWO-DIMENSIONAL WAVE EQUATION

We now consider the wave equation in two dimensions

$$Mu_t + Au_x + Bu_y = 0, \quad (x,y) \in \Omega,\ t \geq 0, \tag{13}$$

where

$$u = \begin{pmatrix} p \\ v_1 \\ v_2 \end{pmatrix},\ M = \begin{pmatrix} K^{-1} & 0 & 0 \\ 0 & \rho & 0 \\ 0 & 0 & \rho \end{pmatrix},\ A = \begin{pmatrix} 0 & 1 & 0 \\ 1 & 0 & 0 \\ 0 & 0 & 0 \end{pmatrix},\ B = \begin{pmatrix} 0 & 0 & 1 \\ 0 & 0 & 0 \\ 1 & 0 & 0 \end{pmatrix}. \tag{14}$$

The system (13) describes the propagation of acoustic waves with pressure $p = p(x,y,t)$, and velocity vector $v = v(x,y,t) = (v_1,\ v_2)$ in a medium characterized by the fluid density

$\rho(x,y) > 0$ and the bulk modulus $K(x,y) > 0$. The same set of equations also describes electromagnetic transverse wave propagation [9]. The energy method applied to (13) leads to

$$\frac{1}{2}\frac{d}{dt}\|u\|_M^2 = -\oint_{\partial\Omega} pv \cdot \hat{n} ds, \tag{15}$$

where $\|u\|_M^2 = \int_\Omega u^T M u dx dy$, $\hat{n}$ is the outward-pointing unit normal associated with the boundary $\partial\Omega$, and ds is the infinitesimal line element. The number and form of the boundary conditions can be determined by following the procedure in section 3. For instance, the boundary condition

$$p - Z\left(v \cdot \hat{n}\right) = r\left[p + Z\left(v \cdot \hat{n}\right)\right], \quad (x,y) \in \partial\Omega, \tag{16}$$

where $Z = \sqrt{\rho K}$, results in an estimate if $|r| \leq 1$.

4.1 The semi-discrete approximation

An SBP-SAT staggered grid approximation of (13) is given by

$$\tilde{M}\mathbf{u}_t + \tilde{A}\mathbf{u} + \tilde{B}\mathbf{u} = \mathbf{BT}_T + \mathbf{BT}_B + \mathbf{BT}_L + \mathbf{BT}_R. \tag{17}$$

In (17), we have introduced

$$\mathbf{u} = \begin{pmatrix} \mathbf{p} \\ \mathbf{v}_1 \\ \mathbf{v}_2 \end{pmatrix}, \ \tilde{M} = \begin{pmatrix} K^{-1} & 0 & 0 \\ 0 & \rho_1 & 0 \\ 0 & 0 & \rho_2 \end{pmatrix},$$

$$\tilde{A} = \begin{pmatrix} 0 & D_{x-} \otimes I_{y-} & 0 \\ D_{x+} \otimes I_{y-} & 0 & 0 \\ 0 & 0 & 0 \end{pmatrix}, \ \tilde{B} = \begin{pmatrix} 0 & 0 & I_{x-} \otimes D_{y-} \\ 0 & 0 & 0 \\ I_{x-} \otimes D_{y+} & 0 & 0 \end{pmatrix},$$

where $\otimes$ denotes the Kronecker product. Here we have chosen to store p at the center of the grid cells (Figure 2). The diagonal matrices K^{-1}, ρ_1, ρ_2 hold the material properties and coincide with the location of p, v_1, v_2, respectively. Furthermore, $I_{x\pm}$ and $I_{y\pm}$ are identity matrices of appropriate sizes.

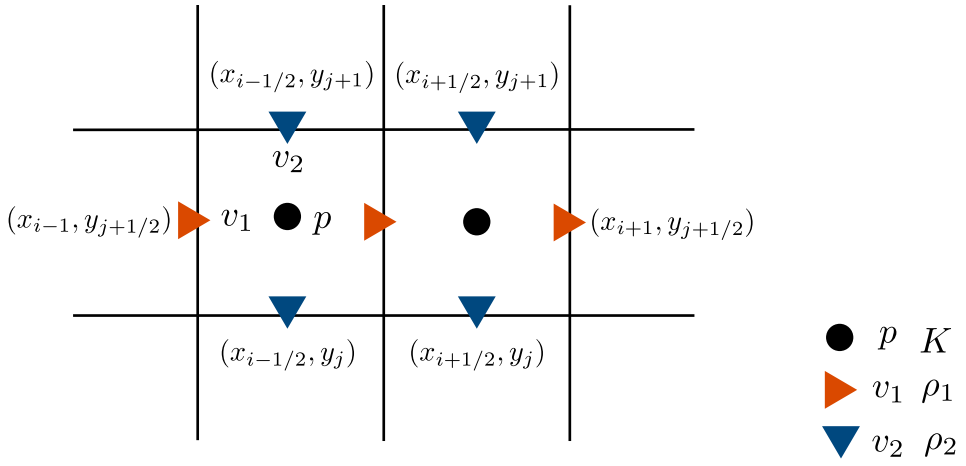

Figure 2: Staggered grid layout for the acoustic wave equation (13).

The boundary condition (16) on the top boundary is weakly imposed by

$$\begin{aligned} \mathbf{BT}_T = P^{-1} E_T P_T \Sigma_T L_T E_T^T \mathbf{u}, \qquad P = \begin{pmatrix} P_{x-} \otimes P_{y-} & 0 & 0 \\ 0 & P_{x+} \otimes P_{y-} & 0 \\ 0 & 0 & P_{x-} \otimes P_{y+} \end{pmatrix}, \\ P_T = \begin{pmatrix} P_{x-} & 0 & 0 \\ 0 & P_{x+} & 0 \\ 0 & 0 & P_{x-} \end{pmatrix}, \quad E_T = \begin{pmatrix} I_{x-} \otimes \mathbf{e}_{y_N-} & 0 & 0 \\ 0 & I_{x+} \otimes \mathbf{e}_{y_N-} & 0 \\ 0 & 0 & I_{x-} \otimes \mathbf{e}_{y_N+} \end{pmatrix}. \end{aligned} \tag{18}$$

The penalty matrix and boundary operator related to (18) are given by

$$\Sigma = \frac{1}{2} \begin{pmatrix} -Z^{-1} \\ \hat{n}_1 \\ \hat{n}_2 \end{pmatrix}, \; L(r) = \begin{pmatrix} 1-r \\ -Z\hat{n}_1 \left(1+r\right) \\ -Z\hat{n}_2 \left(1+r\right) \end{pmatrix}^T, \tag{19}$$

where Σ_T and L_T in (18), are obtained by inserting the unit normal on the boundary $\hat{n} = (0, \; 1)^T$ into (19).

5 NUMERICAL EXPERIMENTS

We test the accuracy of the SBP staggered scheme by using a manufactured solution. The SBP staggered scheme are compared against SBP nodal schemes of the same order for wave propagation over long times. Finally, we demonstrate that the SBP staggered scheme can accurately propagate waves generated by a singular source term acting on the boundary.

In each numerical experiment there is a fundamental wavelength λ that must be resolved. We use λ and the wave speed $c = \sqrt{K/\rho}$ to nondimensionalize (13), assuming constant material properties ($\rho = $ const., $K = $ const.). The dimensionless temporal and spatial scales are given by

$$\bar{t} = kct, \; \bar{x} = kx, \; \bar{y} = ky,$$

where $k = 2\pi/\lambda$. We also nondimensionalize pressure and velocity using

$$\bar{p} = \frac{p}{\rho c V}, \; \bar{v}_1 = \frac{v_1}{V}, \; \bar{v}_2 = \frac{v_2}{V},$$

where V is a reference amplitude. The wave equation (13) in dimensionless form becomes

$$\bar{u}_{\bar{t}} + \bar{A}\bar{u}_{\bar{x}} + \bar{B}\bar{u}_{\bar{y}} = 0, \; \bar{u} \; = \begin{pmatrix} \bar{p} \\ \bar{v}_1 \\ \bar{v}_2 \end{pmatrix}, \; \bar{A} = \begin{pmatrix} 0 & 1 & 0 \\ 1 & 0 & 0 \\ 0 & 0 & 0 \end{pmatrix}, \; \bar{B} = \begin{pmatrix} 0 & 0 & 1 \\ 0 & 0 & 0 \\ 1 & 0 & 0 \end{pmatrix}. \tag{20}$$

Throughout the remainder of the paper we will exclusively use the nondimensional form (20). For notational convenience we will drop the superscript denoting nondimensional variables. In the experiments, we will use the same grid spacing in each coordinate direction $\Delta x = \Delta y$, and advance in time using a 4^{th}-order Runge-Kutta scheme and a sufficiently small time step to make the temporal errors negligible. The error will be measured as $\|\mathbf{u}^{(\Delta x_1)} - \mathbf{u}^*\|_h^2$ where $\mathbf{u}^{(\Delta x)}$ is the numerical solution obtained using the grid spacing Δx and $\mathbf{u}^*$ is computed from an analytic solution, sampled at the grid points.

5.1 Accuracy

To assess the accuracy of the SBP staggered grid operators, we introduce the manufactured solution

$$\begin{aligned} p(x,y,t) &= \sin(x+y+\sqrt{2}t), \\ v_1(x,y,t) &= -\frac{1}{\sqrt{2}}\sin(x+y+\sqrt{2}t), \\ v_2(x,y,t) &= -\frac{1}{\sqrt{2}}\sin(x+y+\sqrt{2}t) \end{aligned} \tag{21}$$

The computational domain is the square $\Omega = (0,\ 2\pi m) \times (0,\ 2\pi m)$, where $m = 10$ (number of wavelengths). The numerical boundary condition is imposed by setting $r = 0$ in (16) and using the manufactured solution (21) as boundary data. The numerical solution is advanced in time until $t = 2\pi m$ and is resolved using $2\pi/\Delta x = 6.4$ grid points per wavelength on the coarsest grid. For numerical schemes constructed using nodal SBP operators the convergence rate is expected to be $s+1$, where $2s$ is the interior accuracy [10]. Figure 3 shows that the SBP staggered scheme converges at this rate or higher.

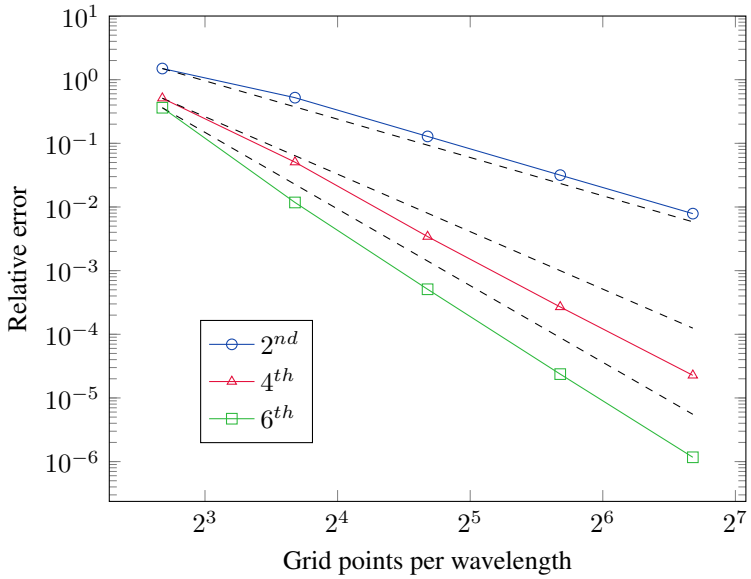

Figure 3: Error in the numerical solution computed using SBP staggered grid operators for the test problem (21). The dashed lines show reference convergence rates $s = 2, 3, 4$, respectively.

5.2 Dispersion error

To assess the dispersion error of the SBP staggered grid operators, we introduce the manufactured solution

$$\begin{aligned} p(x,y,t) &= \sin(x)\sin(y)\cos(\sqrt{2}t), \\ v_1(x,y,t) &= -\frac{1}{\sqrt{2}}\cos(x)\sin(y)\sin(\sqrt{2}t), \\ v_2(x,y,t) &= -\frac{1}{\sqrt{2}}\sin(x)\cos(y)\sin(\sqrt{2}t), \end{aligned} \tag{22}$$

defined on the computational domain $\Omega = (0,\ 2\pi m) \times (0,\ 2\pi m)$, where $m = 16$ (the number of wavelengths). The manufactured solution (22) satisfies the boundary condition $p = 0$ on all of the boundaries. The numerical boundary condition is imposed by setting $r = -1$ in (19). For this boundary condition the continuous energy is conserved. Therefore solution is trapped inside the computational domain, causing the error to grow in time. This test will also confirm that the implementation is stable by integrating over long times.

We compare the performance of the 6^{th}-order SBP staggered and nodal grid operators using $2\pi/\Delta x \approx 16$ grid points per wavelength, and advance until the final time $t \approx 10^4$, which requires nearly 5×10^4 time steps. The relative error growth in time of the SBP staggered and nodal schemes is shown in Figure 4. In a practical calculation, it is useful to define an error threshold that denotes the maximum relative error that can be tolerated. If the maximum error is $\epsilon = 0.05$, then the SBP staggered and nodal schemes reach this threshold after about $t = 4775$ and $t = 616$, respectively. This test clearly demonstrates the superior accuracy of the SBP staggered grid operators.

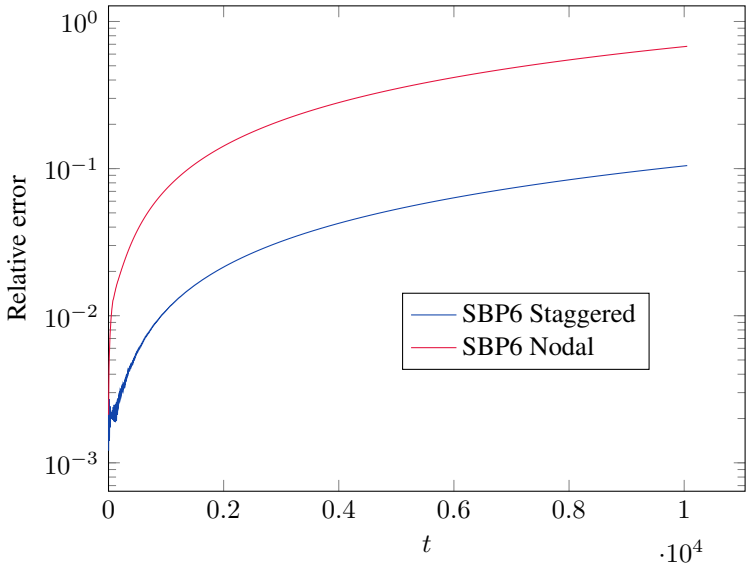

Figure 4: Error growth in time for the test problem (22) using 16 grid points per wavelength.

5.3 An additional capability

A staggered grid difference method offers the ability to discretize a singular source term without introducing any spurious oscillations. We will confirm that the new SBP staggered grid operators also possess this property.

On the top boundary, we specify the boundary condition $p = g(t)\delta(x - x_*)$, where $g(t)$ is the Ricker wavelet function

$$g(t) = (1 - 2\pi^2 f_0^2 (t - t_0)^2) e^{-\pi^2 f_0^2 (t - t_0)^2}, \tag{23}$$

and $\delta(x)$ is the Dirac delta function. The Dirac delta function is defined by

$$\int_{-\infty}^{\infty} f(x)\delta(x - x_*)dx = f(x_*), \tag{24}$$

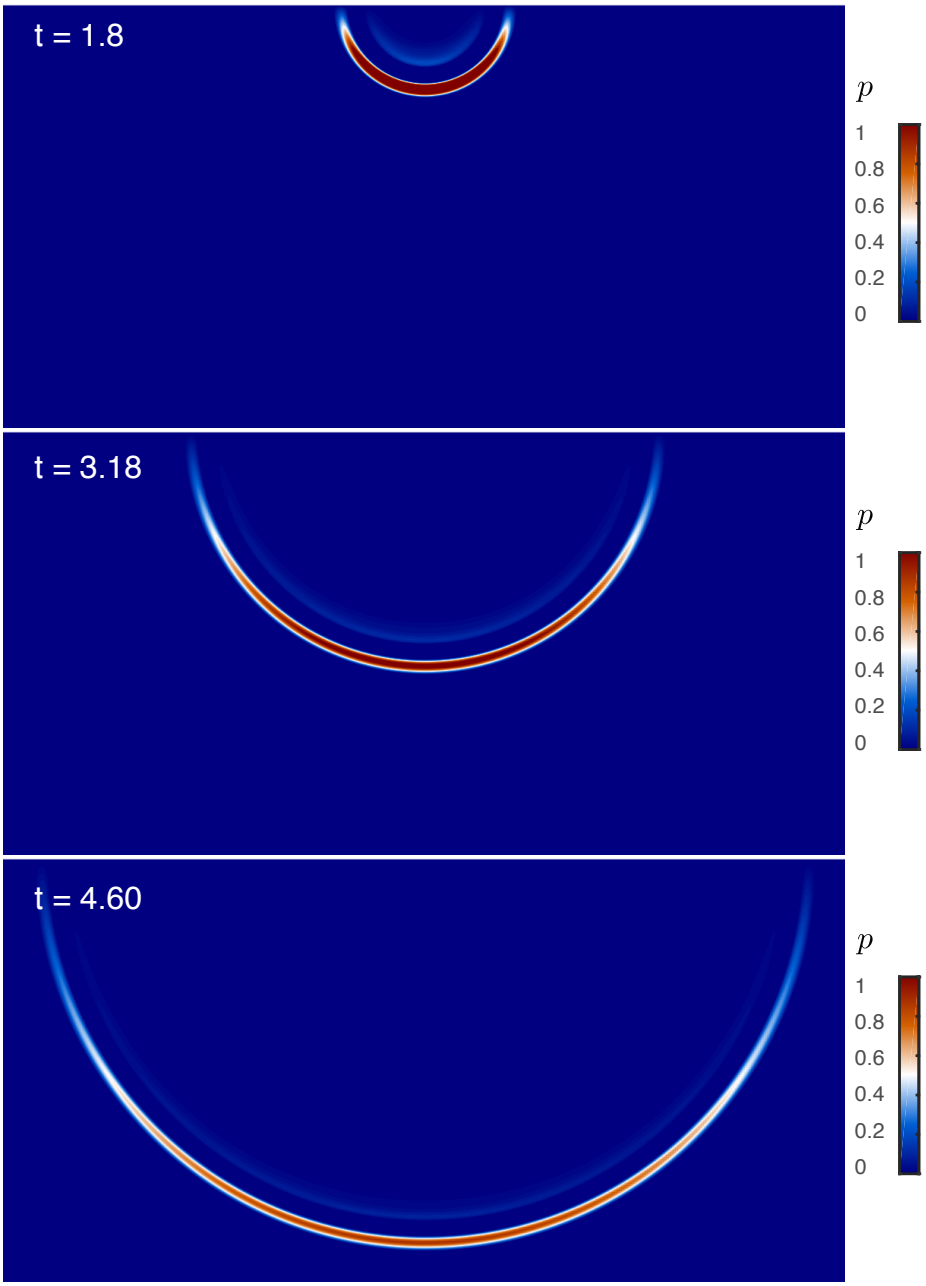

Figure 5: The normalized pressure wave field generated by a singular source term placed in the middle of the top boundary. The simulation uses 6 grid points per minimum wavelength and the 6^{th}-order SBP staggered grid operators. Note that only positive values of p are shown.

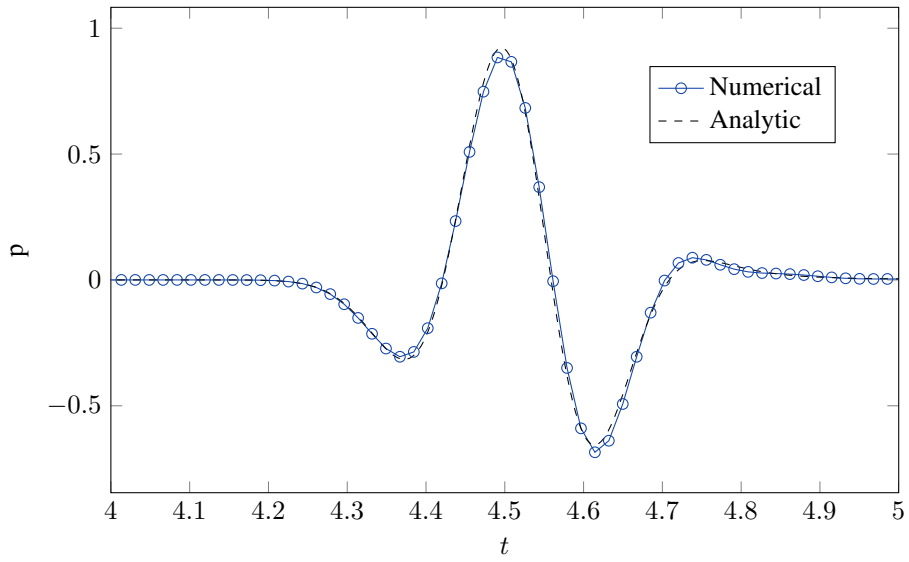

Figure 6: The numerical solution obtained at a fixed point in space 26 minimum wavelengths away from the source. The simulation uses 6 grid points per minimum wavelength and the 6^{th}-order SBP staggered grid operators.

for some function $f(x)$. We approximate (24) by

$$\sum_{j=0}^{N} d_j f(x_j) \approx f(x_*), \tag{25}$$

where the sum is taken over N grid points and the weights d_j at each grid point x_j are determined such that (25) is an accurate approximation of (24). If the source location x_* coincides with a grid point x_l, then the following approximation is commonly used

$$d_j = \begin{cases} \frac{1}{\Delta x}, & j = l, \\ 0, & j \neq l. \end{cases}$$

Otherwise, if x_* is not located exactly on a grid point, then the approximation (26) will be 1^{st}-order accurate. We store the discretization of the delta function at the cell-centered grid points along the top boundary in the vector $\mathbf{d} = \left(d_0,\, d_{1/2},\, \ldots,\, d_{N-1/2},\, d_N\right)^T$ and set the source location to the grid point in the middle of the boundary. The boundary condition is implemented by

$$\mathbf{B}\mathbf{T}_T = P^{-1} E_T P_T \Sigma_T L_T (r = -1) \left(E_T^T \mathbf{u} - g(t)\mathbf{e}\right),\ \mathbf{e} = (\mathbf{d},\, \mathbf{0},\, \mathbf{0})^T,$$

where the dimensionless penalty matrix Σ_T and boundary operator L_T are determined by (19).

We use the 6^{th}-order SBP staggered grid operators with $2\pi/\Delta x \approx 6$ grid points per minimum wavelength. The minimum wavelength λ_{min} is defined by the maximum frequency f_{max} above which the spectral amplitude becomes less than 5% of the maximum value associated with the fundamental frequency f_0 of the Ricker wavelet (23) [4]. The maximum frequency is estimated as $f_{max} \approx 2.5 f_0$. Thus, $\lambda_{min} = 1/f_{max}$ since the wave equation has been nondimensionalized. Figure 5 shows the pressure wave field at different instances in time. We also compare the numerical solution against an analytic solution at a fixed point 26 minimum wavelengths away from the source (Figure 6). The numerical solution is in very good agreement with the analytic solution. The maximum error in amplitude is $\approx 4\%$.

6 CONCLUSIONS

We have extended the SBP-SAT methodology to staggered grids. The general procedure was outlined for both the wave equation in one dimension and two dimensions. The accuracy of the scheme was investigated using a smooth analytic solution. A test with a singular source term on the boundary was used to show that the SBP boundary modification did not destroy the excellent dispersion properties of staggered grid difference methods. Due to the generality of the SBP-SAT methodology, the work can easily be extended to other types of wave equations.

Acknowledgement

We thank Eric M. Dunham for many helpful discussions. Eric M. Dunham derived the analytic solution used in the final numerical experiment.

REFERENCES

[1] Gustafsson, B. and Kreiss, H.O. and Oliger, J, *Time dependent problems and difference methods*. Wiley-Interscience, 1995.

[2] M.H. Carpenter,D. Gottlieb, and S. Abarbanel, Time-stable boundary conditions for finite-difference schemes solving hyperbolic systems: Methodology and application to high-order compact schemes, *Journal of Computational Physics*, **111**, 220, 1994.

[3] B.Strand, Summation by parts for finite difference approximations for d/dx *Journal of Computational Physics*,**110**,47, 1994.

[4] Dimitri Komatitsch and Jean-Pierre Vilotte, The spectral element method: an efficient tool to simulate the seismic response of 2D and 3D geological structures, *Bulletin of the seismological society of America*, **88-2**,368-392, 1998,

[5] Zingg, David W, Comparison of high-accuracy finite-difference methods for linear wave propagation, *SIAM Journal on Scientific Computing*, **22-2**,476-502, 2000.

[6] Nordström, Jan and Carpenter, Mark H, High-order finite difference methods, multidimensional linear problems, and curvilinear coordinates, *Journal of Computational Physics*, **173-1**, 149-174, 2001.

[7] Nordström, Jan and Björck, Martin, Finite volume approximations and strict stability for hyperbolic problems, *Applied numerical mathematics*, **38-3**,237-255, 2001.

[8] Hesthaven, Jan S, High-order accurate methods in time-domain computational electromagnetics: A review, *Advances in imaging and electron physics*, **127**, 59-125, 2003.

[9] Nordström, Jan and Gustafsson, Rikard, High order finite difference approximations of electromagnetic wave propagation close to material discontinuities, *Journal of Scientific Computing*, **18-2**, 215-234, 2003.

[10] Svärd, Magnus and Nordström, Jan On the order of accuracy for difference approximations of initial-boundary value problems, *Journal of Computational Physics*, **218-1**, 333-352, 2006.

[11] Svärd, Magnus and Nordström, Jan, Review of summation-by-parts schemes for initial–boundary-value problems, *Journal of Computational Physics*, **268**,17-38,2014.

[12] Nordström, Jan, Well Posed Problems and Boundary Conditions in Computational Fluid Dynamics, *22nd AIAA Computational Fluid Dynamics Conference, at Dallas, Texas, USA*, 2015.